ADVANCED ELECTRONIC MATERIALS
www.advelectronicmat.de

Omnidirectional Stretchable Inorganic-Material-Based Electronics with Enhanced Performance

Yogeenth Kumaresan, Hyeonghun Kim, Yusin Pak, Praveen Kumar Poola, Ryeri Lee, Namsoo Lim, Heung Cho Ko, Gun Young Jung, and Ravinder Dahiya**

Inorganic material-based devices are well known for their high performance, excellent stability, and hence suitability for fast computation and communication. But their nonflexibility and nonstretchability often hinder their application in several emerging areas where conformability with irregular 3D surfaces is required in addition to the high performance. Herein, with honeycomb like patterns, the omnidirectional stretchability and conformability of inorganic material-based device are demonstrated without sacrificing the performance. The simple method presented here facilitates the transfer of patterned inorganic material-based devices from rigid poly(methyl methacrylate) (PMMA)/glass substrate onto flexible/stretchable substrate such as polydimethylsiloxane simply by placing a water droplet at the PMMA/glass interface. As a proof of concept, the intrinsically brittle indium–gallium–zinc oxide (IGZO)-based stretchable photodetector devices are fabricated. These devices can be stretched up to 10% without performance degradation, which is a significant improvement considering the less than ≈1% fracture limit of IGZO. With Au decoration, these devices show 127-fold higher responsivity (295.3 mA W^{-1}) than planar IGZO devices. The higher fracture strain together with the omnidirectional stretchability underpinned by the honeycomb pattern could allow presented devices to conform to complex hemispherical surfaces such as the human eyes, thus showing significant potential for future high-performance stretchable electronics.

1. Introduction

The flexible electronic devices such as transistors, supercapacitors, photodetectors, solar cells, and various types of sensors,[1] have driven advances in several domains including robotics,[2] smart artificial skin or electronic skin (eSkin),[3] wearable electronics,[4] and health monitoring.[5] With complex arrangements such as stretchable photodetectors on hemispherical surfaces,[6] it is possible to explore new opportunities such as mimicking the biological eye for improved vision in robots. As a result the electronic devices capable of both bending and stretching have been explored using different forms of materials, [7] structures,[8] and innovative fabrication processes.[9] Generally, the stretchability and/or conformability have been attained either by utilizing inherently stretchable devices[10] or through stretchable interconnects (intrinsically stretchable conductors).[11,8c] The former approach relies on elastomeric semiconductor composites that show good elasticity.[10] However, their poor environmental stability and low carrier mobility are some of the issues which need to be resolved. In the latter approach, the electronic devices are fabricated on the rigid substrates (using the traditional methods and high-performance inorganic semiconductors and metals to retain the device functionalities) and stretchable interconnects are utilized to enable the stretchability. However, the stretchability of most of the interconnects are limited to uniaxial direction.[12] Further, an accidental stress on the rigid platform could still deteriorate the device functionality and soldering of device and interconnects is not robust. In this regard, the intrinsically stretchable devices directly made from high performance inorganic material could offer interesting solutions.

The structural design of nonstretchable inorganic materials have been broadly utilized to realize stretchable inorganic electronic devices or device arrays.[13] For example, the wavy geometry of the metal oxide, created by transferring or depositing a thin metal oxide layer onto the prestretched elastomeric substrate, could facilitate the stretchability.[14] Alternatively, thin metal oxide layers could be connected by various stretchable structures such as serpentine, zigzag, fractal-inspired designs, etc., to achieve island–bridge configuration.[9b,15] However, complicated fabrication process, low yield, and difficulties in terms of device handling with aforementioned techniques makes these approaches more challenging.[13a] The ability of conventional inorganic materials to stretch more than their fractal strain (<1%), without performance degradation,[16] lies in the way they are patterned. In

Dr. Y. Kumaresan, Prof. R. Dahiya
University of Glasgow
533a James Watt (South) Building, Glasgow G12 8QQ, UK
E-mail: Ravinder.Dahiya@glasgow.ac.uk
H. Kim, Dr. P. K. Poola, Dr. R. Lee, Dr. N. Lim, Prof. H. C. Ko, Prof. G. Y. Jung
Gwangju Institute of Science and Technology, 261 Cheomdan-gwagiro Buk-gu, Gwangju 500-712, Republic of Korea
E-mail: gyjung@gist.ac.kr
Dr. Y. Pak
Sensor System Research Center (SSRC)
Korea Institute of Science and Technology (KIST)
Seoul 02792, Republic of Korea
The ORCID identification number(s) for the author(s) of this article can be found under https://doi.org/10.1002/aelm.202000058.

DOI: 10.1002/aelm.202000058

this regard, the honeycomb structure, inspired by nature, yields better results than many other geometries, owing to its mechanical stability while stretching.[17] In fact, the stretchable organic transistors have been reported on honeycomb grid perylene substrate.[18] However, the inorganic materials demonstrate superior performance than the organic counterparts, owing to their high carrier mobility and long-term stability under harsh electrical and environmental conditions.[19] The similar honeycomb geometries for stretchable devices based on inorganic materials are yet to be realized. It is challenging to obtain honeycomb-patterned inorganic materials on elastomeric substrate. This is notwithstanding the successful demonstration of the transfer of some metal mesh structures from rigid to the stretchable substrate. As an example, a metal nanomesh structure fabricated on sacrificial K_2SiO_3 layer/Si substrate was transferred to the elastomeric substrate after selectively removing the sacrificial layer in the dilute hydrofluoric acid (HF) solution.[20] In principle such methods could be used for inorganic material-based stretchable device too, but they are not recommended because of potential damage due to HF. Therefore, new fabrication technique is needed to realize intrinsically stretchable inorganic devices.

Herein, we introduce a simple technique to fabricate honeycomb-patterned gold and indium–gallium–zinc oxide (IGZO)-based photodetector device and transfer them onto elastomeric substrate without using any sacrificial layer. The conductive metal mesh, consisting of honeycomb-patterned gold, resting on the poly(methyl methacrylate) (PMMA)/glass substrate is transferred to the elastomeric substrate along with PMMA through exploiting and engineering the surface energy between the PMMA and the glass. The omnidirectional stretchability of honeycomb-patterned gold electrode was studied in terms of the change in resistance while stretching along the zigzag and armchair directions. As a proof of concept, intrinsically stretchable honeycomb-patterned photodetector device, consisting of patterned gold electrode and IGZO active matrix was obtained on stretchable polydimethylsiloxane (PDMS) substrate.

2. Results and Discussion

Figure 1 depicts the fabrication scheme for honeycomb-patterned stretchable gold–IGZO-based photodetector on a thin PMMA layer/glass slide and the subsequent separation of the electrode/devices from the glass slide. An optical image of honeycomb-patterned gold electrode and digital image of honeycomb-patterned IGZO-photodetector array, on PMMA substrate after peeling it off from the underlying glass slide, and their schematic representations are shown in Figure 1b,c, respectively. The detailed explanation of the device fabrication and separation is given in the Experimental Section. We fabricated two different electrodes, namely thin film Au and the honeycomb-patterned Au, on top of PDMS substrate. The fabrication of honeycomb-patterned Au directly onto the PDMS substrate is challenging as its super hydrophobicity hinders the adhesion of photoresist (PR) onto PDMS surfaces while creating a mesh patterns using lithography. Therefore, we fabricated the honeycomb-patterned Au on thin PMMA layer/glass slide and then engineered the surface energy at the interface between

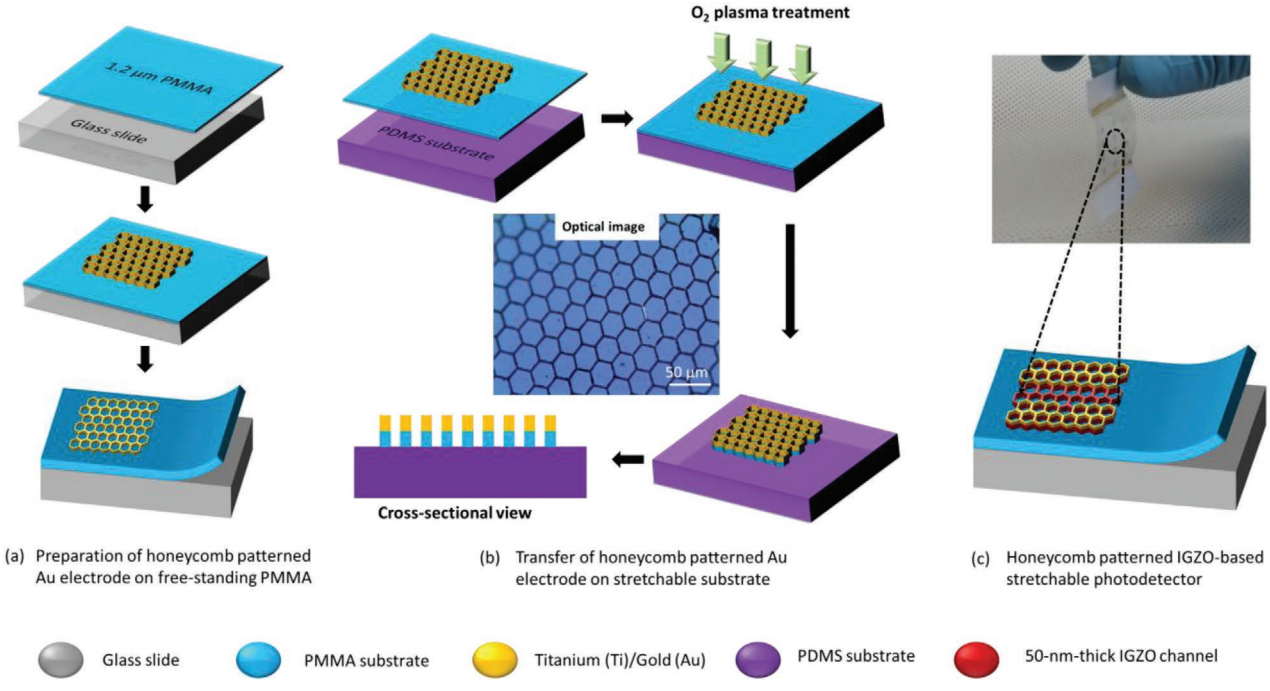

Figure 1. The schematic fabrication process for honeycomb-patterned stretchable gold and IGZO-based stretchable photodetector on ultrathin PMMA substrate. a) Honeycomb-patterned Au on PMMA (detailed fabrication scheme given in Figure S9 in the Supporting Information), b) transfer of honeycomb-patterned Au to PDMS and subsequent O_2 plasma etching of exposed PMMA, and c) honeycomb-patterned IGZO-based stretchable photodetector (detailed fabrication process scheme given in Figure S10 in the Supporting Information). Optical image of honeycomb-patterned Au and digital image of honeycomb-patterned IGZO-based photodetector on PMMA substrate are given in the middle of (b) and top of (c), respectively.

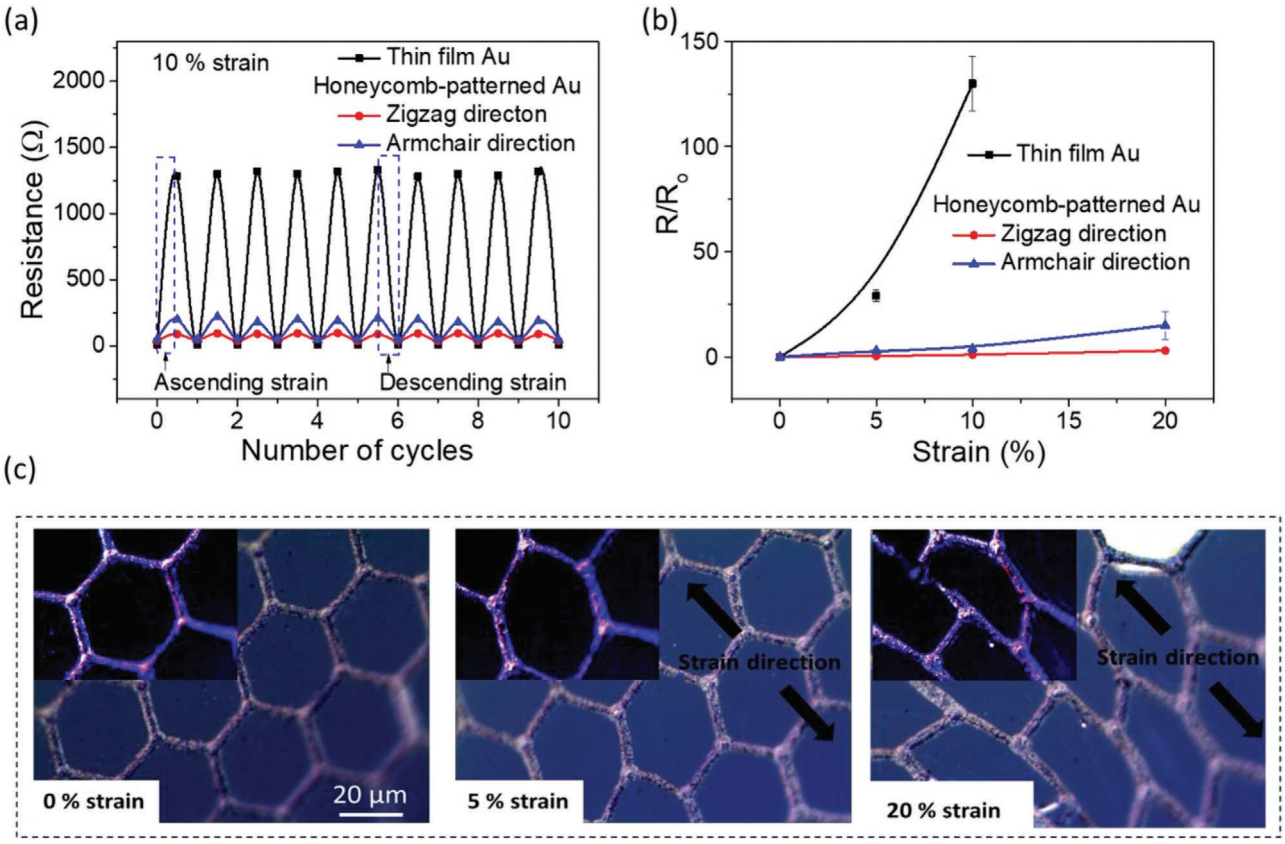

Figure 2. Comparison of electrical performance of thin film Au and the honeycomb-patterned Au while stretching. a) Resistance variation under cyclic stretching at 10% strain, b) change in resistance under different strains, and c) optical image of the honeycomb-patterned Au while stretching along the zigzag direction and their respective magnified images in the inset.

PMMA and a glass substrate to separate the 1.2 μm thick spin-coated PMMA layer, on which the honeycomb-patterned gold mesh structure resided. In our previous work,[21] we found that there were no chemical interactions at the interface between the PMMA layer and unmodified glass slide and this results in easy separation with a drop of water at the interface between PMMA/glass slide (Video S1, Supporting Information). Accordingly, the honeycomb-patterned Au electrode along with thin PMMA layer was transferred to the PDMS substrate and was subjected to further stretching study after removing the exposed PMMA using O_2 plasma treatment.

The stretchability of honeycomb-patterned Au is compared with the thin film Au electrode and the ratio of change in resistance with respect to the strain is plotted in **Figure 2**. Cyclic strain was applied by varying the strain value from 0% to 10% for 10 cycles as shown in Figure 2a. The ratio of change in resistance (R/R_o) for Au thin film increases dramatically while stretching, and the electrode is completely broken (resistance in kΩ) when the strain value goes beyond 10%. On the other hand, the honeycomb-patterned Au demonstrated omnidirectional stretchability above 10% strain, along the zigzag and armchair directions, and the ratio of change in resistance is negligible in comparison with the thin film electrode, as shown in Figure 2b. The resistance could be calculated by using the formula $R = \rho L/A$ where, R is the resistance, ρ is resistivity of Au, L is the length of the Au, and A is the area of connected path of Au.[22] Accordingly, the resistance value increases when there is a crack/discontinuity in the gold connection path. The honeycomb-patterned gold exhibits microcracks when stretched at 20% along the armchair direction (Figure S1, Supporting Information). However, no visible cracks were observed when it was stretched along the zigzag direction (Figure 2c), which led to lower change in resistance in comparison with stretching in armchair direction as shown in Figure 2,b. When the sample was subjected to higher strain (25% and 30%) along the armchair direction, the R/R_o increased dramatically (Figure S2, Supporting Information), with the value of resistance changing from ≈40 to ≈3000 Ω at 30% strain. In addition, the resistance value did not restore to its original value and stayed at ≈1200 Ω after releasing the strain (Figure S2b, Supporting Information). This is because of emergence of few random cracks with >20% stretching (Figure S2c, Supporting Information), when the geometry of Au electrode is converted from honeycomb to rectangular, while stretching along the zigzag direction. Further straining resulted in peeling off of honeycomb-patterned Au from the underlying PMMA/PDMS (Figure S2d, Supporting Information), which resulted in increased resistance due to the discontinuity in the gold connection path and making it more difficult to reach the pristine resistance value even after releasing the strain (Figure S2b, Supporting Information). However, the honeycomb-patterned gold which are stretched <20%, could easily restore to its pristine resistance

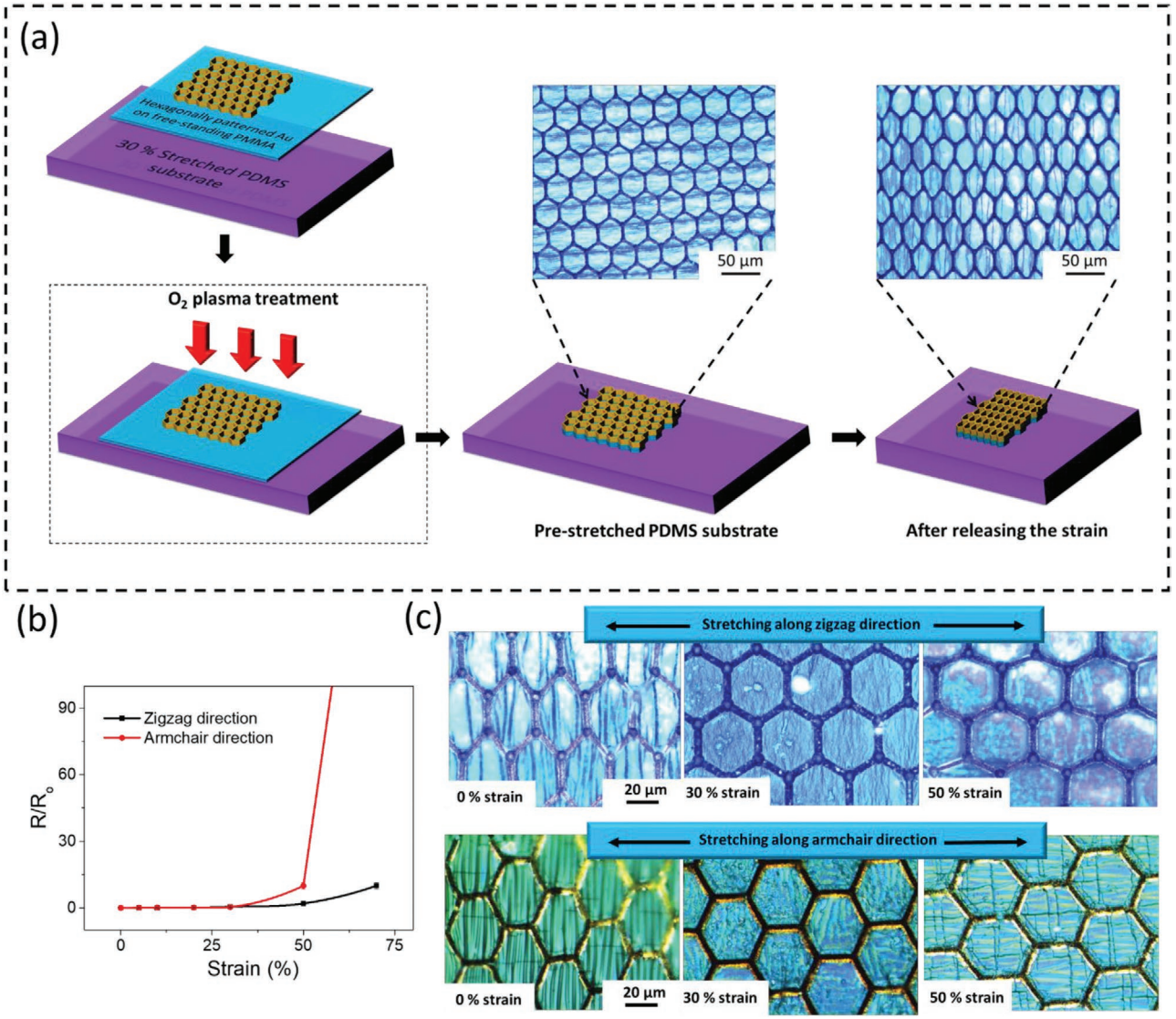

Figure 3. Fabrication and characterization of honeycomb-patterned Au placed on the prestretched PDMS substrate. a) A schematic drawing representing the transfer process of honeycomb-patterned stretchable Au electrode on prestretched PDMS and their respective optical images, b) change in resistance under different strain, and (c) optical image while stretching along the zigzag direction and the armchair direction.

value after releasing the strain and maintained similar performance for 10 manual stretching cycles as shown in Figure 2b. Based on these observations, we conclude that the honeycomb-patterned Au could be effectively used for up to 20% stretchability while the thin film Au could not resist. To enhance the stretchability of honeycomb-patterned Au, the patterned Au was transferred to a 30% prestretched PDMS substrate as shown in **Figure 3**. Prior to the transfer of honeycomb Au electrode onto PDMS, the oxygen plasma treatment was performed to enhance the adhesion. Oxygen plasma treatment introduces polar functional group such as Si–OH which changes the surface of PDMS to hydrophilic with smaller water contact angle (<20°).[23] The smaller contact angle of PDMS indicates that it had a higher surface energy.[21] The thermoplastic polymers such as PMMA interacts with –OH group of PDMS to achieve improved bonding.[24] Subsequently, the honeycomb pattern was transferred to the prestretched PDMS substrate and the plasma treatment was performed under prestretched state to remove the exposed PMMA as shown in Figure 3a (inside dotted box). After releasing the strain, the geometry is changed to compressed honeycomb geometry as shown in the optical image of Figure 3a (top right corner). Interestingly, there are no visible cracks, even at 1000× magnification, on the compressed honeycomb geometry (Figure S3, Supporting Information).

The electrical test under stretching was used to confirm the performance enhancement of compressed honeycomb-patterned Au electrode placed on prestretched PDMS substrate; the ratio of change in resistance is less than 10, while stretched along both the zigzag and armchair direction, under 50% strain as shown in Figure 3b. As the PDMS substrate was prestretched, the original honeycomb geometry was obtained at 30% strained (Figure 3c). Accordingly, the honeycomb geometry

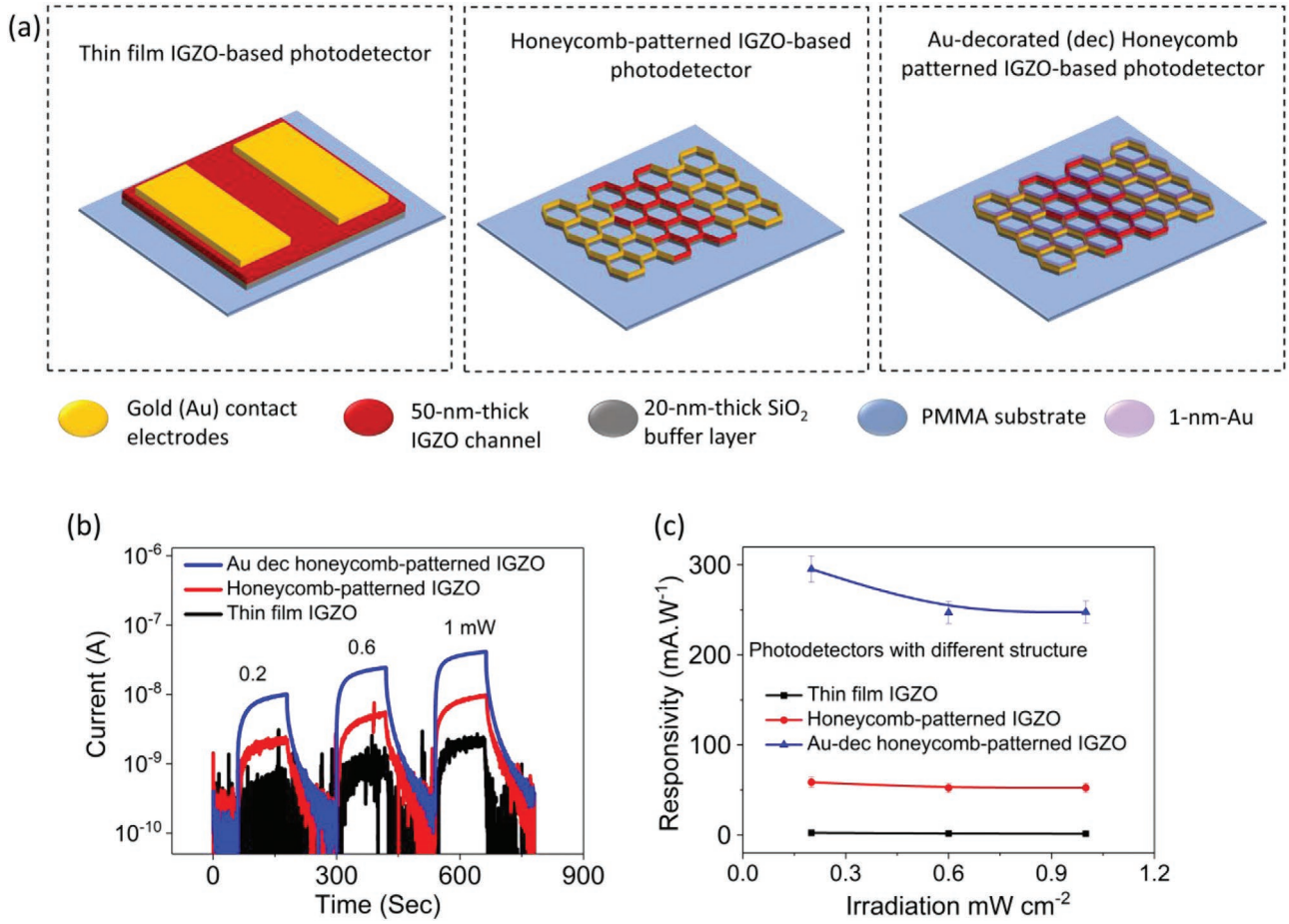

Figure 4. Comparison of three different photodetector devices, namely, thin film-based photodetector, honeycomb-patterned IGZO-based photodetector, and Au-decorated (Au-dec) honeycomb-patterned IGZO-based photodetector. a) Schematic representation of three different photodetectors, b) time-resolved photoresponse under different irradiations, and c) their respective responsivity.

faced a compressive strain below 30% and tensile strain above 30%. Interestingly, the honeycomb-patterned Au electrode on prestretched PDMS substrate reveals two times higher stretchability than the honeycomb-patterned Au electrode on normal PDMS, which makes it a potential candidate for electrodes in the wearable inorganic devices.

In order to study the effect of honeycomb pattern on the metal oxide-based devices, namely, IGZO-based photodetector device, we fabricated three photodetector devices, with the plain IGZO channel, honeycomb-patterned IGZO channel, and 1 nm Au decorated honeycomb-patterned IGZO channel. The schematic diagrams of these photodetectors are shown in **Figure** 4a. The fabrication processes of the photodetector devices are explained in the Experimental Section. The time-resolved photoresponses of photodetector devices on PMMA substrate were measured under different irradiation (0.2 to 1 mW cm^{-2} at a fixed wavelength (365 nm)) and bias voltage (5 V) as shown in the Figure 4b. All the photodetectors exhibit a low dark current value around ≈0.1 nA under the absence of the UV irradiation. In the presence of UV irradiation, an abrupt increase in the current level was observed in all the devices due to the generation of electron–hole pairs in the IGZO and the current value saturates at some level and then gradually decreases after the UV irradiation is turned off (Figure 4b). In dark condition, the oxygen species in the air ambient acts as an electron acceptor, which are physically and/or chemically adsorbed onto the IGZO surface in the absence of UV irradiation. It captures the free electrons present in the IGZO channel [O_2 (g) + e^- → O_2^- (ad)], and results in the formation of electron depletion regions, thus decreasing the conductivity of IGZO channel.[25] When the IGZO channel is illuminated by a 365 nm UV-light the electron–hole pairs are photogenerated [hν → h^+ + e^-] and the electrons move to the conduction band of IGZO channel and are pushed to the contact electrode by the applied bias. The hole reacts with the physically and/or chemically adsorbed oxygen species, discharge the absorbed oxygen ions [h^+ + O_2^- (ad)→ O_2 (g) + e^-], and release the chemisorbed electrons back into the IGZO channel. Therefore, the electron carrier density increases within the IGZO channel, resulting in an increase in the conductivity. Both the electron–hole pairs generation and the oxygen absorption/desorption on the surface of the IGZO are responsible for the UV light sensing. The outer surface of the IGZO is responsible for more electron–hole pair generation due to the exponential decay of irradiation intensity inside the materials. This is owing to the absorption coefficient of the material, which results in decreased electron–hole pair

Table 1. The value of responsivity and external quantum efficiency (EQE) of three photodetector devices at 0.2 mW cm^{-2} irradiation.

Device type (area) [cm^2]	Power [mW cm^{-2}]	Photocurrent (I_{ph}) − dark current (I_d) ($I_{ph} - I_d$) [mA]	Power × area ($P \cdot A$) [W]	Responsivity $\left(R_\lambda = \frac{I_{ph} - I_d}{P \cdot A}\right)$ [mA W^{-1}]	EQE $= \frac{hc}{e\lambda} R_\lambda$ [%]
Plain IGZO (16×10^{-4})	0.2	7.44×10^{-7}	3.2×10^{-7}	2.325	0.78
Honeycomb-patterned IGZO (16.24×10^{-5})	0.2	1.9×10^{-6}	3.25×10^{-8}	58.5	19.890
Au decorated honeycomb-patterned IGZO (16.24×10^{-5})	0.2	9.6×10^{-6}	3.25×10^{-8}	295.3	100.5

generation underneath the surface in comparison with the outer surface (Figure S4, Supporting Information). In patterned geometry, the area of the outer surface of IGZO exposed to the irradiation is much larger in comparison with the nonpatterned geometry (Figures S4-1,3 and S5, Supporting Information). Accordingly, in our study the active outer surface area of IGZO exposed to UV light is much larger for the honeycomb-patterned IGZO (1.13×10^7 μm^2) than the planar IGZO (1.6×10^5 μm^2) (Figure S5, Supporting Information). Therefore, two honeycomb-patterned IGZO-based photodetector devices exhibited better sensor response and responsivity (Figure 4b,c). As shown in **Table 1**, the responsivity of the honeycomb-patterned IGZO (58.5 mA W^{-1}) is 25 times higher than the planar IGZO (2.325 mA W^{-1}) with a high external quantum efficiency (EQE) of 19.89% (the responsivity and EQE calculations are given as a table in Figure S6 in the Supporting Information). In general, the intensity of irradiation decays exponentially inside the materials owing to the reflection of incident light due to the index difference which results in decreased electron–hole pair generation underneath the surface. Accordingly, the EQE value, which is the number of electrons detected per incident photon, for larger surface area honeycomb-patterned IGZO-based photodetector device (19.89%) is higher than the planar IGZO (0.78%) as shown in Table 1. Further, the 1 nm Au decoration on honeycomb-patterned IGZO is found to increase the responsivity by more than five times in magnitude, from 58.5 to 295.3 mA W^{-1} at 0.2 mW cm^{-2}, as shown in Figure 4c. This enhanced performance is due to interband transition of Au electrons in the UV regime[26] and/or hole-trapping at Au/IGZO interface.[27] Upon UV illumination, the filled d-band in Au provides large number of electrons for the interband excitation from 5d to 6sp (Figure S7a, Supporting information,).[28] In the presence of applied bias, the excited electrons are transferred to the conduction band of IGZO at Au/IGZO interface resulting in enhanced photoconductivity. Accordingly, the number of generated electrons per incident photon reached the highest value of 100.5% at 0.2 mW cm^{-2} with ≈127-fold higher responsivity than the planar IGZO-based photodetector. To achieve our objective, which is flexibility along with the good device performance in IGZO-based photodetectors, we utilized Au decorated honeycomb-patterned IGZO photodetector, whose responsivity is highest among the three devices, for further stretching studies.

The Au-decorated honeycomb-patterned IGZO on PMMA substrate was transferred to the PDMS and the exposed PMMA was removed by plasma treatment. Two Au-decorated honeycomb-patterned IGZO devices were fabricated and subjected to stretching; one device was stretched along the channel width direction (zigzag direction) and the other device was stretched along the channel length direction (armchair direction) as shown in **Figure** 5a. The digital and respective optical images of the photodetector placed on the stretching tool under 0% and 20% strain along zigzag direction are given in Figure S7b,c in the Supporting Information, respectively. The photoresponse was measured under different stretching conditions varying from 0% to 20% at a fixed UV intensity, wavelength, and bias voltage (1 mW cm^{-2}, 365 nm, 5 V). The photoresponse of the devices remains constant up to 10% strain for zigzag direction and up to 5% strain for armchair direction, but the photocurrent (current under illumination) decreased when the device experienced higher strain as shown in the Figure 5b and the device response is not recovered even after releasing the strain as shown in Figure 5c (Figure S7d, Supporting Information). The responsivity and EQE of the device remain almost constant (260 mA W^{-1} and 88.4%) up to 10% strain along zigzag direction but there is 14-fold decrease in the responsivity and EQE when the device was subjected to 20% strain, as shown in Figure 5d (Figure S7e (table), Supporting Information). Along armchair direction, twofold decrease in the responsivity was observed at 10% strain and an extreme decrease in responsivity (≈30-fold decrease) was observed at 20% strain as shown in Figure 5d. We assume that there might be the formation of numerous cracks/discontinuities at the IGZO channel resulting in the drastic decrease in the responsivity. Even though the honeycomb-patterned gold on the nonstretched PDMS substrate (Figure 2) demonstrated stable performance, the honeycomb-patterned IGZO is broken at 20% strain (for both directions). This is because of the directional nature of stronger ionic bond formed between the metal and oxygen in metal oxides, which makes them brittle while experiencing 20% strain.[29] Contrary to this, the atoms in Au form a metallic bond, which is more likely to deform while stretching. Therefore, the honeycomb-patterned gold electrode demonstrated high stretchability (Figure 2) in comparison with IGZO. In general, the amorphous metal oxides such as IGZO cannot handle more than 1% strain under bending or stretching; interestingly, the honeycomb-patterned IGZO has the potential to handle more than 10% strain. Further, after 100 stretching cycles at 10% strain, the Au decorated honeycomb-patterned IGZO demonstrated stable sensing performance as shown in Figure 5e. There are few reports that utilized metal oxide nanowire network[30] or crumpled graphene + plain graphene hybrid architecture[31] to demonstrate better stretchability but the responsivity of the device is limited to <0.005 mA W^{-1} which is not suitable for good spectral detection.[31] In comparison with the recent reports on IGZO-based photodetectors (Figure S8, Supporting Information),[32] our honeycomb-patterned photodetector demonstrate promising performance in terms of both responsivity and stretchability. In fact, the honeycomb geometry enhanced the device performance and introduced inherent stretchability to the device. These honeycomb photodetectors have the capability to be conformally

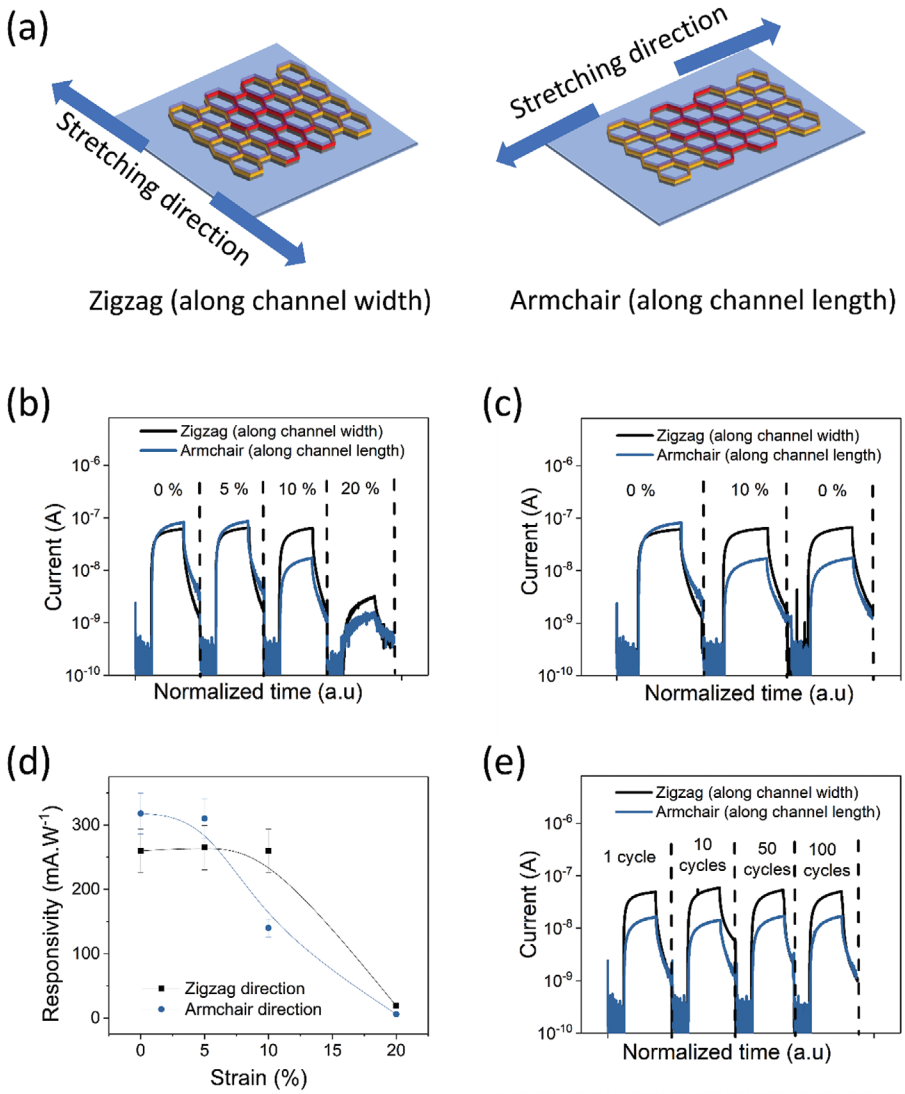

Figure 5. The Au-decorated honeycomb-patterned IGZO-based photodetector stretched along channel length and channel width directions. a) Schematic representation of devices stretched along zigzag and armchair direction. b) Sensing response of photodetector at different stretching conditions, c) under stretching and releasing at 10% strain, and d) their respective responsivity. e) The repeatability tests up to 100 cycles at 10% strain (the response measured after releasing the stretching).

attached to complex concave or convex structure to mimic the human eyes, as the maximum induced strain on the device array conformally attached to the hemispherical eye module is <8%,[33] which is lower than the fracture strain of our device.

3. Conclusion

In conclusion, the omnidirectional stretchable inorganic IGZO-based photodetector devices with stable performance were demonstrated in this manuscript using honeycomb-patterned structures. The honeycomb-patterned gold electrode placed on prestretched PDMS substrate revealed an excellent omnidirectional stretchability up to 50% without considerable change in the resistance. Further, honeycomb-patterned IGZO demonstrated higher responsivity of 58.5 mA W^{-1} at 0.2 mW cm^{-2} in comparison with the planar IGZO (2.325 mA W^{-1}). The 1 nm Au decoration on honeycomb-patterned IGZO further enhanced the responsivity to 295.3 mA W^{-1}. The Au decorated honeycomb-patterned IGZO photodetector device revealed an unprecedented stretchability up to 10% without any performance degradation, indicating a significant advancement toward inorganic semiconductor-based wearable and stretchable electronics.

4. Experimental Section

Figure 1 depicts the schematic flow for the fabrication of honeycomb-patterned inorganic materials, such as Au electrode and IGZO-based photodetector device, on the ultrathin PMMA substrate and transferring them to an elastomeric substrate.

Preparation of Honeycomb-Patterned Au Electrode on Free Standing PMMA: A 1.2 µm thick PMMA layer was spin coated on a rigid glass

slide and annealed at 130 °C for 2 h. A sequence of photolithography, metal deposition, and lift-off processes were performed to obtain the hexagonally patterned Au electrode on PMMA as shown in Figure S9 in the Supporting Information. As the PMMA layer gets affected while stripping the photoresist in acetone, 0.7 µm thick PVA layer was spin coated as a sacrificial layer to make the metal lift-off process feasible on PMMA/glass substrate. Sequentially, 0.1 µm thick back antireflection coating (BARC) and 2.2 µm thick GXR positive PR was spin coated and annealed at 100 and 115 °C for 1 min, respectively. As shown in Figure S9 in the Supporting Information, a sequence of UV exposure, developing, and reactive ion etching (RIE) were performed to obtain a honeycomb trench in PVA/PR. In all the experiments, 20 nm thick SiO_2 was deposited as a barrier layer using electron beam (e-beam) evaporator after RIE process. Then, 5/100 nm thick Ti/Au (SiO_2/Ti/Au collectively named as Au) was deposited using e-beam evaporator. The hexagonally patterned Au was obtained on PMMA/glass after lift-off in deionized (DI) water. Following the fabrication of the hexagonally patterned Au, the PMMA substrate along with the pattern was readily peeled off the rigid glass slide by placing a tiny water drop at the interface between the glass slide and PMMA layer.

Transfer of Hexagonally Patterned Au onto the Elastomeric PDMS Substrate: Prior to the transfer of patterned Au electrode, the PDMS substrate was treated under oxygen plasma using RIE to enhance the adhesion of PMMA with the PDMS substrate. As shown in Figure 1b, oxygen plasma treatment was performed again, after placing the hexagonally patterned Au/PMMA on PDMS substrate, to remove the exposed PMMA region, the region that was uncovered by the Au. The optical image in the middle of Figure 1b shows the hexagonally patterned Au transferred onto the elastomeric PDMS.

Fabrication of IGZO-Based Photodetectors: The honeycomb-patterned IGZO-based photodetector fabrication is explained in Figure S10 in the Supporting Information. As mentioned in the "Preparation of Honeycomb-Patterned Au Electrode on Free Standing PMMA" section, the honeycomb trench in PVA/PR was fabricated using photolithography and RIE process. The 20 nm SiO_2 barrier layer was deposited over the honeycomb trench, followed by the 50 nm thick IGZO layer deposited by RF sputtering using an IGZO (In_2O_3:Ga_2O_3:ZnO = 1:1:1 atomic ratio) target at a base pressure of 3×10^{-6} mbar with Ar:O_2 gas flow rate of 100:2 sccm under a constant chamber pressure of 5 mTorr. Sequentially, the contact electrodes (Ti/Au: 5/50 nm) were deposited using a shadow mask with a channel length and width of 80 µm and 2 mm, respectively. After deposition, the device was placed in water to lift-off PVA along with the deposited metals and semiconductors to achieve honeycomb-patterned IGZO photodetector device. In the case of Au decorated IGZO-based device, the 1 nm Au was deposited over the honeycomb-patterned IGZO-based device using e-beam evaporator without any masks. The planar IGZO photodetector device was fabricated by depositing 20 nm thick SiO_2 and 50 nm thick IGZO using e-beam evaporator and RF sputtering on PMMA/glass. The contact electrodes (Ti/Au: 5/50 nm) were deposited using e-beam evaporation with a shadow mask. As shown in Figure 1c, all the fabricated devices were readily peeled off the rigid glass slide by placing a tiny water drop at the interface between the glass slide and PMMA layer (see Video S1 in the Supporting Information).

Supporting Information

Supporting Information is available from the Wiley Online Library or from the author.

Acknowledgements

This work was supported in part by the Basic Science Research Program (No. NRF- NRF-2019R1A2B5B01070640) through the National Research Foundation of Korea (NRF) funded by the Ministry of Science and ICT. The research was partially supported by the GIST Research Institute (GRI) project through a grant provided by GIST in 2019; the Engineering and Physical Sciences Research Council (EPSRC) through engineering fellowship for growth (EP/R029644/1 and EP/M002527/1) and the European Commission through FET-OPEN project Ph-Coding (H2020-FETOPEN-2018-829186).

Conflict of Interest

The authors declare no conflict of interest.

Keywords

gold electrodes, InGaZnO, lithography, photodetectors, stretchable electronics

Received: January 10, 2020
Revised: March 29, 2020
Published online: May 20, 2020

[1] a) H. Zhang, P. Gutruf, K. Meacham, M. C. Montana, X. Zhao, A. M. Chiarelli, A. Vázquez-Guardado, A. Norris, L. Lu, Q. Guo, C. Xu, Y. Wu, H. Zhao, X. Ning, W. Bai, I. Kandela, C. R. Haney, D. Chanda, R. W. Gereau, J. A. Rogers, *Sci. Adv.* **2019**, *5*, eaaw0873; b) J. Zou, M. Zhang, J. Huang, J. Bian, Y. Jie, M. Willander, X. Cao, N. Wang, Z. L. Wang, *Adv. Energy Mater.* **2018**, *8*, 1702671; c) Y. Jiang, Z. Liu, N. Matsuhisa, D. Qi, W. R. Leow, H. Yang, J. Yu, G. Chen, Y. Liu, C. Wan, Z. Liu, X. Chen, *Adv. Mater.* **2018**, *30*, 1706589; d) L. Manjakkal, C. G. Núñez, W. Dang, R. Dahiya, *Nano Energy* **2018**, *51*, 604; e) M. K. Choi, J. Yang, T. Hyeon, D.-H. Kim, *npj Flexible Electron.* **2018**, *2*, 10; f) S. Nakata, M. Shiomi, Y. Fujita, T. Arie, S. Akita, K. Takei, *Nat. Electron.* **2018**, *1*, 596; g) L. Manjakkal, W. T. Navaraj, C. G. Núñez, R. Dahiya, *Adv. Sci.* **2019**, *6*, 1802251; h) L. Manjakkal, A. Pullanchiyodan, N. Yogeswaran, E. S. Hosseini, R. Dahiya, *Adv. Mater.* **2020**, https://doi.org/10.1002/adma.201907254; i) L. Manjakkal, D. Szwagierczak, R. Dahiya, *Prog. Mater. Sci.* **2020**, *109*, 100635; j) Y. Zhao, A. Kim, G. Wan, B. C. K. Tee, *Nano Convergence* **2019**, *6*, 25; k) C. Parameswaran, D. Gupta, *Nano Convergence* **2019**, *6*, 28; l) A. Zumeit, W. T. Navaraj, D. Shakthivel, R. Dahiya, *Adv. Electron. Mater.* **2020**, *6*, 1901023.

[2] a) R. Dahiya, *Proc. IEEE* **2019**, *107*, 247; b) M. Ntagios, H. Nassar, A. Pullanchiyodan, W. T. Navaraj, R. Dahiya, *Adv. Intell. Syst.* **2019**, *1*, 1900080; c) W. Navaraj, R. Dahiya, *Adv. Intell. Syst.* **2019**, *1*, 1900051; d) R. Dahiya, W. T. Navaraj, S. Khan, E. O. Polat, *Inf. Disp.* **2015**, *31*, 6.

[3] a) H. Tran, V. R. Feig, K. Liu, Y. Zheng, Z. Bao, *Macromolecules* **2019**, *52*, 3965; b) R. Dahiya, N. Yogeswaran, F. Liu, L. Manjakkal, E. Burdet, V. Hayward, H. Jörntell, *Proc. IEEE* **2019**, *107*, 2016; c) O. Ozioko, P. Karipoth, P. Escobedo, M. Ntagios, A. Pullanchiyodan, R. Dahiya, *Adv. Intell. Syst.* **2020**; d) M. Soni, R. Dahiya, *Philos. Trans. R. Soc., A* **2020**, *378*, 20190156; e) C. García Núñez, L. Manjakkal, R. Dahiya, *npj Flexible Electron.* **2019**, *3*, 1.

[4] a) J. Choi, A. J. Bandodkar, J. T. Reeder, T. R. Ray, A. Turnquist, S. B. Kim, N. Nyberg, A. Hourlier-Fargette, J. B. Model, A. J. Aranyosi, S. Xu, R. Ghaffari, J. A. Rogers, *ACS Sens.* **2019**, *4*, 379; b) W. S. Lee, S. Jeon, S. J. Oh, *Nano Convergence* **2019**, *6*, 10.

[5] a) J. Yoon, Y. Joo, E. Oh, B. Lee, D. Kim, S. Lee, T. Kim, J. Byun, Y. Hong, *Adv. Sci.* **2019**, *6*, 1801682; b) M. A. Kafi, A. Paul, A. Vilouras, R. Dahiya, *Biosens. Bioelectron.* **2020**, *147*, 111781; c) M. A. Kafi, A. Paul, A. Vilouras, E. S. Hosseini, R. Dahiya, *IEEE Sens. J.* **2019**, https://doi.org/10.1109/JSEN.2019.2928807.

[6] J. Xue, Z. Zhu, X. Xu, Y. Gu, S. Wang, L. Xu, Y. Zou, J. Song, H. Zeng, Q. Chen, *Nano Lett.* **2018**, *18*, 7628.
[7] a) C. S. Luo, P. Wan, H. Yang, S. A. A. Shah, X. Chen, *Adv. Funct. Mater.* **2017**, *27*, 1606339; b) D. Shakthivel, M. Ahmad, M. R. Alenezi, R. Dahiya, S. R. P. Silva, *1D Semiconducting Nanostructures for Flexible and Large-Area Electronics*, Cambridge University Press, Cambridge **2019**; c) D. Shakthivel, W. T. Navaraj, S. Champet, D. H. Gregory, R. S. Dahiya, *Nanoscale Adv.* **2019**, *1*, 3568; d) F. Liu, W. T. Navaraj, N. Yogeswaran, D. H. Gregory, R. Dahiya, *ACS Nano* **2019**, *13*, 3257.
[8] a) C. Zhang, A. Khan, J. Cai, C. Liang, Y. Liu, J. Deng, S. Huang, G. Li, W.-D. Li, *ACS Appl. Mater. Interfaces* **2018**, *10*, 21009; b) W. Dang, L. Manjakkal, W. T. Navaraj, L. Lorenzelli, V. Vinciguerra, R. Dahiya, *Biosens. Bioelectron.* **2018**, *107*, 192; c) W. Dang, V. Vinciguerra, L. Lorenzelli, R. Dahiya, *Flexible Printed Electron.* **2017**, *2*, 013003.
[9] a) Y. R. Jeong, G. Lee, H. Park, J. S. Ha, *Acc. Chem. Res.* **2019**, *52*, 91; b) K. Park, D.-K. Lee, B.-S. Kim, H. Jeon, N.-E. Lee, D. Whang, H.-J. Lee, Y. J. Kim, J.-H. Ahn, *Adv. Funct. Mater.* **2010**, *20*, 3577; c) C. García Núñez, F. Liu, S. Xu, R. Dahiya, *Integration Techniques for Micro/Nanostructure-Based Large-Area Electronics*, Cambridge University Press, Cambridge **2018**; d) C. García Núñez, W. T. Navaraj, F. Liu, D. Shakthivel, R. Dahiya, *ACS Appl. Mater. Interfaces* **2018**, *10*, 3058.
[10] H.-J. Kim, K. Sim, A. Thukral, C. Yu, *Sci. Adv.* **2017**, *3*, e1701114.
[11] Q. Zhang, J. Liang, Y. Huang, H. Chen, R. Ma, *Mater. Chem. Front.* **2019**, *3*, 1032;
[12] R. Xu, Y. Zhang, K. Komvopoulos, *Mater. Res. Lett.* **2019**, *7*, 110.
[13] a) T. Q. Trung, N.-E. Lee, *Adv. Mater.* **2017**, *29*, 1603167; b) Z. Xue, H. Song, J. A. Rogers, Y. Zhang, Y. Huang, *Adv. Mater.* **2019**, *32*, 1902254; c) X. Zheng, H. Cheng, *Sci. China: Technol. Sci.* **2019**, *62*, 209.
[14] a) D.-Y. Khang, H. Jiang, Y. Huang, J. A. Rogers, *Science* **2006**, *311*, 208; b) H. Cheng, Y. Zhang, K.-C. Hwang, J. A. Rogers, Y. Huang, *Int. J. Solids Struct.* **2014**, *51*, 3113.
[15] a) S. Xu, Y. Zhang, J. Cho, J. Lee, X. Huang, L. Jia, J. A. Fan, Y. Su, J. Su, H. Zhang, H. Cheng, B. Lu, C. Yu, C. Chuang, T.-i. Kim, T. Song, K. Shigeta, S. Kang, C. Dagdeviren, I. Petrov, P. V. Braun, Y. Huang, U. Paik, J. A. Rogers, *Nat. Commun.* **2013**, *4*, 1543; b) H. Lee, G. Lee, J. Yun, K. Keum, S. Y. Hong, C. Song, J. W. Kim, J. H. Lee, S. Y. Oh, D. S. Kim, M. S. Kim, J. S. Ha, *Chem. Eng. J.* **2019**, *366*, 62; c) J. Yun, H. Lee, C. Song, Y. R. Jeong, J. W. Park, J. H. Lee, D. S. Kim, K. Keum, M. S. Kim, S. W. Jin, Y. H. Lee, J. W. Kim, G. Zi, J. S. Ha, *Chem. Eng. J.* **2020**, *387*, 124076.
[16] J. A. Rogers, T. Someya, Y. Huang, *Science* **2010**, *327*, 1603.
[17] a) T. Takahashi, K. Takei, A. G. Gillies, R. S. Fearing, A. Javey, *Nano Lett.* **2011**, *11*, 5408; b) A. J. Wang, D. L. McDowell, *J. Eng. Mater. Technol.* **2004**, *126*, 137.
[18] W. Lee, S. Kobayashi, M. Nagase, Y. Jimbo, I. Saito, Y. Inoue, T. Yambe, M. Sekino, G. G. Malliaras, T. Yokota, M. Tanaka, T. Someya, *Sci. Adv.* **2018**, *4*, eaau2426.
[19] a) Y. Kumaresan, Y. Pak, N. Lim, Y. kim, M.-J. Park, S.-M. Yoon, H.-M. Youn, H. Lee, B. H. Lee, G. Y. Jung, *Sci. Rep.* **2016**, *6*, 37764; b) K. J. Yu, Z. Yan, M. Han, J. A. Rogers, *npj Flexible Electron.* **2017**, *1*, 4.
[20] C. F. Guo, T. Sun, Q. Liu, Z. Suo, Z. Ren, *Nat. Commun.* **2014**, *5*, 3121.
[21] Y. Kumaresan, R. Lee, N. Lim, Y. Pak, H. Kim, W. Kim, G.-Y. Jung, *Adv. Electron. Mater.* **2018**, *4*, 1800167.
[22] B. Zhang, J. Lei, D. Qi, Z. Liu, Y. Wang, G. Xiao, J. Wu, W. Zhang, F. Huo, X. Chen, *Adv. Funct. Mater.* **2018**, *28*, 1801683.
[23] a) S. H. Tan, N.-T. Nguyen, Y. C. Chua, T. G. Kang, *Biomicrofluidics* **2010**, *4*, 032204; b) H. Hillborg, J. F. Ankner, U. W. Gedde, G. D. Smith, H. K. Yasuda, K. Wikström, *Polymer* **2000**, *41*, 6851.
[24] a) Z. Wu, N. Xanthopoulos, F. Reymond, J. S. Rossier, H. H. Girault, *Electrophoresis* **2002**, *23*, 782; b) H. Yu, Z. Z. Chong, S. B. Tor, E. Liu, N. H. Loh, *RSC Adv.* **2015**, *5*, 8377; c) M. E. Vlachopoulou, A. Tserepi, P. Pavli, P. Argitis, M. Sanopoulou, K. Misiakos, *J. Micromech. Microeng.* **2009**, *19*, 015007.
[25] Y. Kumaresan, H. Kim, Y. Jeong, Y. Pak, S. Cho, R. Lee, N. Lim, G. Y. Jung, *IEEE Electron Device Lett.* **2017**, *38*, 1735.
[26] Q. Wang, L. Hu, M. Chen, L. Wu, *RSC Adv.* **2015**, *5*, 103636.
[27] N. Gogurla, A. K. Sinha, S. Santra, S. Manna, S. K. Ray, *Sci. Rep.* **2015**, *4*, 6483.
[28] H. Zhu, X. Chen, Z. Zheng, X. Ke, E. Jaatinen, J. Zhao, C. Guo, T. Xie, D. Wang, *Chem. Commun.* **2009**, 7524.
[29] a) M. H. Cho, H. Seol, A. Song, S. Choi, Y. Song, P. S. Yun, K. Chung, J. U. Bae, K. Park, J. K. Jeong, *IEEE Trans. Electron Devices* **2019**, *66*, 1783; b) M. K. Lee, C. Kim, J. W. Park, E. Kim, M. Seol, J. Park, Y. Choi, S. K. Park, K. C. Choi, *IEEE Trans. Electron Devices* **2017**, *64*, 3189.
[30] C. Yan, J. Wang, X. Wang, W. Kang, M. Cui, C. Y. Foo, P. S. Lee, *Adv. Mater.* **2014**, *26*, 943.
[31] M. Kim, P. Kang, J. Leem, S. Nam, *Nanoscale* **2017**, *9*, 4058.
[32] a) M. Sun, Q. Fang, Z. Zhang, O. Xie, O. Sun, J. Xu, O. Li, T. Ren, Y. Zhang, *ACS Appl. Mater. Interfaces* **2018**, *10*, 8; b) X. Xu, L. Yan, T. Zou, R. Qiu, C. Liu, Q. Dai, J. Chen, S. Zhang, H. Zhou, *ACS Appl. Mater. Interfaces* **2018**, *10*, 44144; c) J. Yu, K. Javaid, L. Liang, W. Wu, Y. Liang, A. Song, H. Zhang, W. Shi, T.-C. Chang, H. Cao, *ACS Appl. Mater. Interfaces* **2018**, *10*, 8102; d) N. Yamada, Y. Kondo, X. Cao, Y. Nakano, *Appl. Mater. Today* **2019**, *15*, 153; e) D. L. Jiang, L. Li, H. Y. Chen, H. Gao, Q. Qiao, Z. K. Xu, S. J. Jiao, *Appl. Phys. Lett.* **2015**, *106*, 171103; f) C.-Y. Huang, M.-L. Chen, C.-W. Yu, T.-C. Wan, S.-H. Chen, C.-Y. Chang, T.-Y. Hsu, *Nanotechnology* **2018**, *29*, 505202; g) H. K. Li, T. P. Chen, S. G. Hu, X. D. Li, Y. Liu, P. S. Lee, X. P. Wang, H. Y. Li, G. Q. Lo, *Opt. Express* **2015**, *23*, 27683; h) H. T. Zhou, L. Li, H. Y. Chen, Z. Guo, S. J. Jiao, W. J. Sun, *RSC Adv.* **2015**, *5*, 87993.
[33] C. Choi, M. K. Choi, S. Liu, M. S. Kim, O. K. Park, C. Im, J. Kim, X. Qin, G. J. Lee, K. W. Cho, M. Kim, E. Joh, J. Lee, D. Son, S.-H. Kwon, N. L. Jeon, Y. M. Song, N. Lu, D.-H. Kim, *Nat. Commun.* **2017**, *8*, 1664.